2015 IEEE International Conference on Robotics and Automation (ICRA)
Washington State Convention Center
Seattle, Washington, May 26-30, 2015

Designing Snap-Free Concentric Tube Robots: A Local Bifurcation Approach

Richard J. Hendrick, *Student Member, IEEE*, Hunter B. Gilbert, *Student Member, IEEE* and Robert J. Webster III, *Senior Member, IEEE*

***Abstract*— In designing concentric tube robots, it is often desirable to use curvatures that are as high as possible. However, with high curvatures comes the potential for elastic instabilities. This can be addressed by motion planning or by designing the robot to preclude the possibility of instability. In this paper, we pursue the latter. Our primary contribution is to show that local bifurcation theory can be used to predict the existence of elastic instability anywhere in the workspace of robots with arbitrarily many tubes, with straight transmissions. We show how to use these results to design robots that are guaranteed to remain elastically stable at all times.**

I. Introduction

When the elastic, precurved tubes that make up a concentric tube robot are rotated and translated with respect to one another, the tubes elastically interact, storing strain energy. During normal operation, the strain energy in the backbone (i.e. the collection of tubes) changes in a continuous, smooth fashion, creating smooth motions of the curved robot. However, for robots with sufficiently high precurvatures in their tubes, there will be configurations in which elastic energy is suddenly released and the robot "snaps" rapidly from one configuration to another.

It has previously been noted that snapping of concentric tube robots is an essential area of future work [1]–[3]. Snapping can be handled in two ways: one can design robots that have no snaps in their workspace by choosing appropriate tube parameters, or one can use a set of tubes that does exhibit snapping and ensure elastic stability through motion planning or control. The latter approach was recently taken in [4], where stable paths were planned by continuously checking the relative twist between the base of a tube and its tip for all tube rotations in a tube set. However, to date most design algorithms have not taken snapping into account [1], [5]–[7], leaving it to future work.

This material is based upon work supported by the the National Institutes of Health under R01 EB017467 and the National Science Foundation under CAREER award IIS-1054331 and two Graduate Research Fellowships DGE-0909667. Any opinions, findings, and conclusions or recommendations expressed in this material are those of the authors and do not necessarily reflect the views of the National Institutes of Health or the National Science Foundation.

The authors wish to acknowledge Noah Cowan, who suggested linearization as a means to characterize snapping behavior over five years ago, and Gabor Kosa who separately suggested several years ago that perturbation analysis might be valuable in this problem. It took us this long to realize and demonstrate that both these insights were correct.

R. J. Hendrick, H. B. Gilbert, and R. J. Webster III are with the Vanderbilt Department of Mechanical Engineering, Vanderbilt University, Nashville, TN USA, {richard.j.hendrick, hunter.b.gilbert, robert.webster}@vanderbilt.edu

The purpose of this paper is to provide a computationally efficient test for a given design, which will enable the designer to immediately determine whether snapping will occur anywhere in the robot's workspace. This test (Algorithm 2) can be used to quickly eliminate from consideration potentially large areas of the available design space when seeking a snap-free design. Such a test could be useful when designing robots to reach specific points [6], designing robots for optimal surgical site coverage [1], designing robots to pass through confined areas such as tubular structures [8], and designing robots with desired workspace properties [9].

The snapping problem in concentric tube robots was first studied in [10] and [11], using the transmissional torsion model (which neglects torsion in the curved sections of the device). As the mechanics-based model matured and became more accurate by including torsion in curved sections, as well as general precurvatures [12], [13], it was no longer clear how to predict snapping.

Recently, an analytic approach to designing snap-free robots was proposed in [3], in which exact bounds for two tubes and conservative bounds for more than two tubes were defined. When more than two tubes are present, the results in [3] apply when the component tube precurvatures are precisely aligned in arc length. Contributions in this paper beyond [3] are (1) to derive results that are exact for any number of tubes, (2) to provide results that apply to any configuration of the robot, and (3) to analyze the problem using local bifurcation theory.

Physical tube modifications can also enhance stability of a concentric tube robot, as shown in [14] and [15]. In these papers, the tubes were laser machined to reduce the ratio of bending to torsional stiffness, which reduces torsional strain energy storage. However, even using this approach, snaps will still occur if sufficiently high curvatures are employed, so methods for snap prediction are still needed. Another design-based approach was shown in [16] where non-constant tube precurvatures were used to enhance the elastic stability of a planar two-tube robot. Our paper differs in that we restrict our elastic stability analysis to circularly precurved tubes with straight transmissions, and we apply the analysis to concentric tube robots composed of arbitrarily many tubes.

To date, the snapping problem has not been analyzed using bifurcation theory. Bifurcation theory lends itself well to the snapping problem since it is designed to capture abrupt changes in solution structures as parameters vary [17], which is precisely what happens when a concentric tube robot

snaps. Local bifurcation theory, which is often utilized in Euler beam buckling problems, studies the local, linearized behavior of systems around equilibrium points, which is where structural changes in the solution often originate.

In this paper, we show that the type of bifurcation concentric tube robots exhibit is a supercritical pitchfork bifurcation. We derive exact expressions for the location of bifurcation points for robots composed of an arbitrary number of tubes, including straight transmission sections. We show that bifurcations create a non-unique map from actuation space to configuration space and show that avoiding bifurcations guarantees elastic stability. Lastly, we show how to use these bifurcation results to design snap-free concentric tube robots.

II. Mathematical Preliminaries

A. Bifurcation Theory

To define and describe bifurcation, we adopt a general set of mathematical definitions, based on [18]. Let $\boldsymbol{\lambda} \in \mathbb{R}^n$ be a vector of parameters and $\boldsymbol{x}(t) : \mathbb{R} \to \mathbb{R}^n$ be a vector-valued function. In general, $\boldsymbol{x}$ may be required to satisfy certain algebraic conditions (e.g. boundary conditions). Consider an operator, possibly nonlinear, $f[\boldsymbol{\lambda}, \boldsymbol{x}]$, which generates the problem

$$f[\boldsymbol{\lambda}, \boldsymbol{x}] = 0. \tag{1}$$

An equilibrium, $\boldsymbol{x}(t) = \boldsymbol{x}_e$, is a fixed point that solves (1) for all $\boldsymbol{\lambda}$ (we may also refer to this as a trivial solution). The trivial branch of an equilibrium is the set of all points $(\boldsymbol{\lambda}, \boldsymbol{x}_e)$. A point $(\boldsymbol{\lambda}_0, \boldsymbol{x}_e)$ on a trivial branch is called a bifurcation point on this branch if and only if in every neighborhood of this point there is a solution pair $(\boldsymbol{\lambda}_0, \boldsymbol{x})$ with $\boldsymbol{x} \neq \boldsymbol{x}_e$. From this definition, it is clear that the concepts of non-uniqueness and bifurcation are connected.

In a nonlinear system, it is often assumed that the small solutions of its linearization are an accurate representation of the nonlinear problem, but this is not guaranteed, as shown in [18]. One, however, is guaranteed to get useful information about the nonlinear problem by linearizing about an equilibrium point (i.e a trivial configuration). It can be shown that the linear operator defined by the linearization of (1) about $\boldsymbol{x}_e$ will not have a bounded inverse at a bifurcation point $(\boldsymbol{\lambda}_0, \boldsymbol{x}_e)$. This motivates our search for non-trivial solutions to the linearized problem, a process which is sometimes referred to as the criterion of adjacent equilibrium. It is also known for many bifurcation problems that the onset of sudden, unstable, snapping phenomenon (e.g. buckling, snapping, etc.) can be predicted by analyzing only trivial, equilibrium configurations, which is what we find for our problem. For a mathematically rigorous discussion of this approach, see [17], [18].

B. Concentric Tube Robot Model Equations

In this paper, we consider concentric tube robots that operate in free space, and consist of tubes with constant cross section that each have an initial straight section and a circularly precurved tip as shown in Fig. 1. We note that in

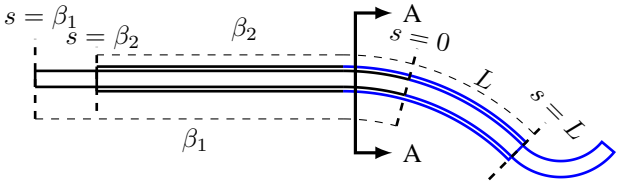

Fig. 1: This diagram illustrates arc length parameter definitions. The blue lines indicate a precurved portion of the tube. We define $s = 0$ as the most proximal point where the precurved sections of both tubes interact. Note that $\beta_1, \beta_2 \leq 0$.

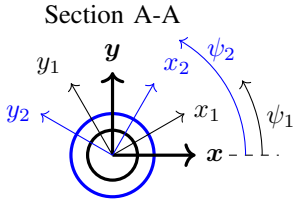

Fig. 2: Each tube has a material-attached frame which propagates along the arc length s of the robot with its z-axis tangent to the backbone of the robot. The absolute rotational angle ψ_i of tube i is measured with respect to a zero-torsion Bishop frame and changes in arc length if the tube is in torsion.

principle all analyses in this paper could apply to planar, non-circular precurvatures, but assuming circular precurvature here at the beginning will simplify the equations and match the majority of concentric tube robots built to date. Advanced models of concentric tube robots are available in [12], [13], and a review of the modeling history for these robots can be found in [2].

The shape of a robot in free space is determined by the solution to the model of the evolution of torsion in arc length s along the tubes:

$$(k_{it}\psi_i')' = \frac{k_{ib}}{k_b}\sum_{j=1}^{n} k_{jb}\kappa_i\kappa_j \sin(\psi_i - \psi_j), \quad k_b = \sum_{l=1}^{n} k_{lb}. \tag{2}$$

The $()'$ operator indicates differentiation with respect to arc length s. ψ_i is the absolute material orientation about the backbone axis of tube i, with respect to a backbone Bishop frame as shown in Fig. 2. k_{it} is the torsional stiffness of tube i, k_{ib} is the bending stiffness of tube i, κ_i is the precurvature of tube i, and n is the number of tubes. The sums are computed over the tubes present in that portion of the backbone (see [19] for this particular form of the equation). This model assumes the system is frictionless.

At the proximal end of a tube, where it is held, ψ_i is fixed (ψ_i will vary in arc length along the tube, but its initial condition is set by the actuator that grasps it), while at the distal tip of each tube there is no torsional moment. Therefore, equation (2) must obey the boundary conditions,

$$\psi_i(0) = \alpha_i - \beta_i\psi_i'(0), \quad (k_{it}\psi_i')(l_i) = 0, \tag{3}$$

where α_i is the actuator rotation of tube i, l_i is the arc length where tube i terminates, and $\beta_i \leq 0$ is the arc length where tube i is held (see Fig. 1). In the proximal boundary condition, it is assumed that the torsion is constant for any $s \leq 0$. Typically, $s = 0$ is defined as the constrained point

where the tubes exit the actuation unit, but $s = 0$ can be chosen at any arc length such that $(k_{it}\psi_i')' = 0$ for all $s \leq 0$, and here we define it as shown in Fig. 1. It is convenient to reduce the dimensionality of our system by expressing the model in terms of relative angles between the local material frames, thus we define $\theta_i = \psi_i - \psi_1$. This reduces the set of torsional angle variables from n to $(n-1)$ since θ_1 is treated as a reference.

III. The Two Tube Case

For $n = 2$, we have that $\theta = \psi_2 - \psi_1$ (we drop the subscript in this section). It will prove convenient to nondimensionalize the arc length, s, by the length of the backbone where both tubes are present and precurved, L. We define $\sigma = s/L$ and choose $\sigma = 0$ as the minimum arc length at which the precurved portions of both tubes overlap. For our initial analysis, let the transmission lengths of each tube be equivalent (i.e. $\beta_1 = \beta_2 = \beta$, we will relax this assumption later). Using operator notation consistent with (1), the nondimensionalized system is

$$\begin{aligned} f[\lambda, \theta(\sigma)] &= \theta'' - \lambda \sin(\theta) = 0 \\ \theta(0) &= \alpha_2 - \alpha_1 - \beta_\sigma \theta'(0) \\ \theta'(1) &= 0, \end{aligned} \tag{4}$$

where $\beta_\sigma = \beta/L$. The bifurcation parameter λ is given by

$$\lambda = L^2 \kappa_1 \kappa_2 \frac{k_{1b}}{k_{1t}} \frac{k_{2b}}{k_{2t}} \frac{k_{1t} + k_{2t}}{k_{1b} + k_{2b}}, \tag{5}$$

which simplifies to $\lambda = L^2 \kappa_1 \kappa_2 (1 + \nu)$ if the tube cross sections are annular and made from the same material, where ν is Poisson's ratio. Note that this simplification does not require each tube to be of the same stiffness. Equation (4) is the two point boundary value problem we will analyze for the remainder of this section.

A. The Bifurcation Diagram for Two Tubes

The notion of the the trivial branch and bifurcation points are challenging concepts to visualize. For concentric tube robots, the concept of the S-Curve, shown in Fig. 3, was first proposed in [12]. When $\lambda < \frac{\pi^2}{4}$ this function maps the relative material orientation at the proximal end of the tubes to the the relative material orientation at the distal end. The difference between these values is driven by torsional strain energy storage in the tubes. If $\lambda \geq \frac{\pi^2}{4}$, the mapping $\theta(0) \rightarrow \theta(1)$ ceases to be a function, with the loss of uniqueness initially occurring at $\theta(0) = \pi$, $\lambda = \frac{\pi^2}{4}$. The loss of uniqueness is apparent on the S-Curve, but the notion of a trivial branch or a bifurcation point cannot be visualized on this diagram.

To address this, we propose to use a bifurcation diagram. A bifurcation diagram can be generated from (4) by plotting points $(\lambda, \theta(1))$. To draw the diagram, the equilibria of (4) must be considered, which are $\theta_e = \alpha_2 - \alpha_1 = 0, \pi$. Not surprisingly, no bifurcation point occurs on the $\theta_e = 0$ trivial branch, since this corresponds to the tube precurvature directions being aligned.

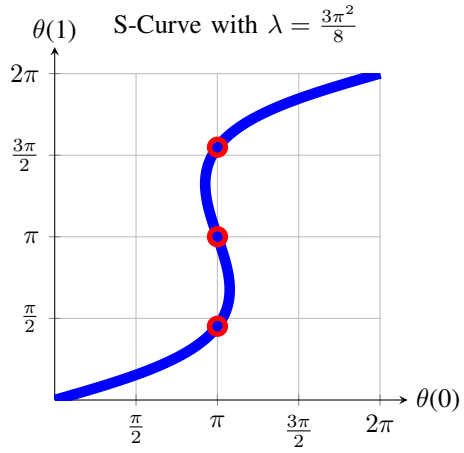

Fig. 3: The S-Curve maps the the proximal relative angle, $\theta(0)$, to the distal relative angle, $\theta(1)$. The red circles show corresponding points in the bifurcation diagram in Fig. 4.

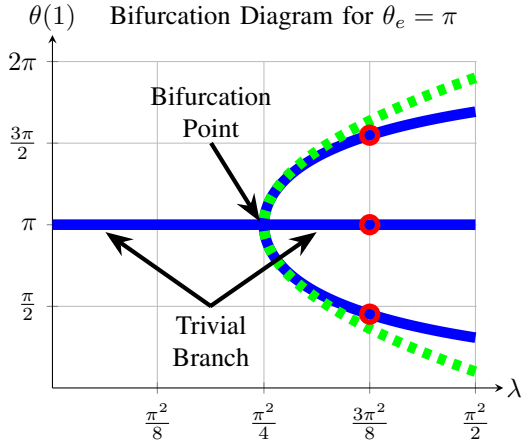

Fig. 4: The bifurcation diagram shows nontrivial branches originating at the bifurcation point $\lambda = \pi^2/4$ when $\beta = 0$. The circles show corresponding points between the bifurcation diagram and the S-Curve in Fig. 3. The green dotted line shows the bifurcation equation solution from (6).

On the other hand, the $\theta_e = \pi$ equilibrium (i.e. when the tube precurvature directions are opposite one another) does bifurcate as seen in Fig. 4. The trivial branch $\theta_e = \pi$ is the only solution when $\lambda < \frac{\pi^2}{4}$ (assuming $\beta = 0$) and can be physically understood as a smooth exchange from bending/torsional energy (when $\theta(0) < \pi$) to only bending energy when $\theta(0) = \pi$. However, when $\lambda \geq \frac{\pi^2}{4}$ non-trivial solution branches emerge. In this case, rather than smoothly transferring the accumulated torsional strain energy to bending energy at $\theta(0) = \pi$, the tubes instead continue to accumulate torsional energy as $\theta(0)$ proceeds past π, until the energy builds to the point that they snap rapidly to another configuration. The snap occurs when the slope of the S-Curve from Fig. 3 is infinite.

This type of bifurcation, which is also seen in the Euler beam buckling problem, is known as a supercritical pitchfork bifurcation because the bifurcation only occurs for values equal to or greater than a critical bifurcation parameter. A local bifurcation equation, which gives the linearized equations of the non-trivial branches near a bifurcation point,

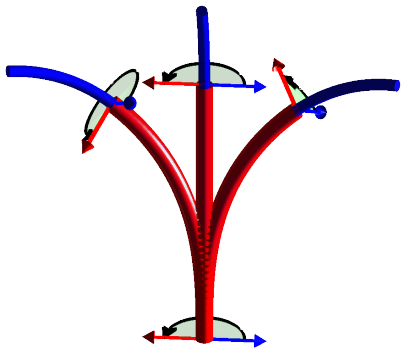

Fig. 5: This figure illustrates the three solutions to the kinematics when $\lambda = 3\pi^2/8$ and $\theta(0) = \pi$ (i.e. when the tube precurvatures are anti-aligned at the base). The arrows indicate the direction of precurvature of each tube given by the right-hand rule, shown at $s = 0$ and $s = 1$. These three configurations correspond to the three solutions shown by the circles in Fig. 3 and Fig. 4. The tubes shown here have equal stiffness, and thus the combined tube set is straightened out in the trivial solution.

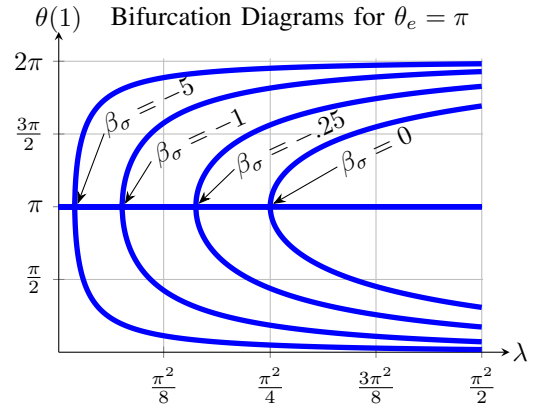

Fig. 6: Bifurcation diagrams are shown for various transmission lengths. As the transmission length grows, the critical bifurcation parameter is reduced.

can be derived for (4) using perturbation methods (see derivation and detailed discussion in the context of beam buckling in [18]) at $\lambda_0 = \frac{\pi^2}{4}$

$$\theta(1) = \pi \pm 2\sqrt{2}\sqrt{\frac{\lambda - \lambda_0}{\lambda_0}}, \quad \lambda \geq \frac{\pi^2}{4}. \tag{6}$$

The bifurcation diagram shows that, for the actuator input of $\theta(0) = \pi$, three configurations of the concentric tube robot exist when $\lambda \geq \lambda_0$ (see Fig. 5 when $\lambda = 3\pi^2/8$). The trivial branch is unstable, and hence is not possible for physical prototypes to achieve, while each of the non-trivial branches are realizable (the configuration seen depends on the actuation history). We also see from Fig. 4 that when when $\lambda < \lambda_0$, a unique solution exists, and therefore, if the design ensures that λ always stays in this realm, the robot will be snap-free. We follow this approach of finding non-trivial solutions near equilibrium configurations in analyzing a variety of more general cases throughout the remainder of the paper.

B. Local Bifurcation Analysis

1) Equal Transmission Lengths: The linearization of (4) at $\theta_e = \pi$ is

$$\theta'' + \lambda(\theta - \pi) = 0, \tag{7}$$

and the general solution is

$$\theta(\sigma) = C_1 \cos(\sqrt{\lambda}\sigma) + C_2 \sin(\sqrt{\lambda}\sigma) + \pi.$$

This solution is subject to the boundaries $\theta(0) = \pi - \beta_\sigma \theta'(0)$ and $\theta'(1) = 0$. Evaluating the proximal boundary, we have that $C_1 = -\beta_\sigma \sqrt{\lambda} C_2$, and plugging this relationship into the distal boundary condition gives $C_2[\beta_\sigma \sqrt{\lambda} \sin(\sqrt{\lambda}) + \cos(\sqrt{\lambda})] = 0$. When $C_2 = 0$, we get the trivial solution $\theta(\sigma) = \theta_e = \pi$, but another, non-trivial solution can be found if the bracketed quantity goes to zero. Therefore, a bifurcation point exists at (λ_0, π) where λ_0 obeys

$$\beta_\sigma = \frac{-\cot(\sqrt{\lambda_0})}{\sqrt{\lambda_0}}. \tag{8}$$

When $\beta_\sigma = 0$, this simplifies to $\lambda_0 = \frac{\pi^2}{4}$, the well-known result for two tubes with no transmission lengths. Thus, the addition of transmission length reduces the critical bifurcation parameter, as illustrated in Fig. 6.

Furthermore, if $\lambda < \lambda_0$, then the design is snap-free, since the design will always remain subcritical. Note that equation (8) is found in a different form in [3] as an inequality that, if satisfied, guarantees a unique solution to the state-linearized model.

2) Unequal Transmission Lengths: In physical concentric tube robot prototypes, the straight transmission lengths will not be equal since smaller tubes must be longer than larger tubes in order to be grasped by their respective actuators. If an equivalent transmission length, $\beta_{eq,\sigma} = f(\beta_{1,\sigma}, \beta_{2,\sigma})$, can be found such that the proximal boundary remains unchanged from (4), the results from the previous section will remain valid for this case.

The proximal boundary condition with differing transmission lengths is $\theta(0) = \alpha_2 - \alpha_1 - \beta_{2,\sigma}\psi_2'(0) + \beta_{1,\sigma}\psi_1'(0)$. Using torsional equilibrium, which must be satisfied along the entire backbone, we can relate $\psi_1'(0)$ and $\psi_2'(0)$: $k_{1t}\psi_1' + k_{2t}\psi_2' = 0$. By combining torsional equilibrium with the definition of θ, the relationship between $\psi_2'(0)$ and $\theta'(0)$ is $\psi_2'(0) = (\frac{k_{1t}}{k_{1t}+k_{2t}})\theta'(0)$. This enables re-expression of the proximal boundary condition in the same form as (4): $\theta(0) = \alpha_2 - \alpha_1 - \beta_{eq,\sigma}\theta'(0)$, where

$$\beta_{eq,\sigma} = \frac{\beta_{1,\sigma}k_{2t} + \beta_{2,\sigma}k_{1t}}{k_{1t} + k_{2t}}. \tag{9}$$

Thus, any two tube robot with unequal transmission lengths can be equivalently represented as two tubes with equal transmission lengths using (9), and the results from the previous section hold.

IV. The Several Tube Case

A. Equal Transmission Lengths

For the several tube case, it is simpler not to nondimensionalize. We start by assuming that the precurved portions of the tubes are fully overlapped with length L (this restriction will be removed later, but eases initial exposition) and each

have the same transmission length, gripped at arc length $\beta \leq 0$. We can express (2) in terms of relative angles as

$$\begin{aligned} \theta_i'' &= \sum_{j=1}^{n} \mathbf{\Phi}_{ij} s_{ij} + \mathbf{\Phi}_{1j} s_j \\ \theta_i(0) &= \alpha_i - \alpha_1 - \beta \theta_i'(0) \\ \theta_i'(L) &= 0, \end{aligned} \tag{10}$$

where $s_i = \sin(\theta_i)$, $s_{ij} = \sin(\theta_i - \theta_j)$, and $\mathbf{\Phi}$ is an $n \times n$ matrix with each entry, Φ_{ij}, defined as

$$\mathbf{\Phi}(i,j) = \kappa_i \kappa_j \frac{k_{ib} k_{jb}}{k_b k_{it}}. \tag{11}$$

Let $\boldsymbol{\theta}_e \in \mathbb{R}^{n-1}$ be an equilibrium point of (10), and linearizing (10) at the equilibrium gives

$$\boldsymbol{\theta}'' = \mathbf{A}_e(\boldsymbol{\theta} - \boldsymbol{\theta_e}), \quad \mathbf{A}_e = \left.\frac{\partial \boldsymbol{\theta}''}{\partial \boldsymbol{\theta}}\right|_{\boldsymbol{\theta}=\boldsymbol{\theta}_e} = \left.\mathbf{A}\right|_{\boldsymbol{\theta}=\boldsymbol{\theta}_e}. \tag{12}$$

$\mathbf{A}$ can be derived from (10) and is given by

$$\mathbf{A}(p-1, q-1) = \begin{cases} \Phi_{1q} c_q + \displaystyle\sum_{j=1, j\neq p}^{n} \Phi_{pj} c_{pj} & (p = q) \\ -\Phi_{pq} c_{pq} + \Phi_{1q} c_q & (p \neq q) \end{cases} \tag{13}$$

where $c_i = \cos(\theta_i)$, $c_{ij} = \cos(\theta_i - \theta_j)$, and the indices $p, q = 2, \ldots, n$ (we omit the trivial equation $\theta_1 = 0$).

To express (12) in first-order form, we define the state vector, $\boldsymbol{x}$, and equilibrium state, $\boldsymbol{x}_e$, as $\boldsymbol{x}^T = \begin{bmatrix} \boldsymbol{\theta} & \boldsymbol{\theta}' \end{bmatrix}$, $\boldsymbol{x}_e^T = \begin{bmatrix} \boldsymbol{\theta}_e & \mathbf{0} \end{bmatrix}$, such that (12) becomes

$$\boldsymbol{x}' = \underbrace{\begin{bmatrix} 0 & I \\ \mathbf{A}_e & 0 \end{bmatrix}}_{\tilde{\mathbf{A}}_e} (\boldsymbol{x} - \boldsymbol{x}_e). \tag{14}$$

$\mathbf{A}_e$ can be decomposed into its eigendecomposition[1] as $\mathbf{A}_e = \mathbf{V}\mathbf{\Lambda}\mathbf{V}^{-1}$, and we can rewrite (14) equivalently as

$$\underbrace{\begin{bmatrix} \mathbf{V}^{-1} & \mathbf{0} \\ \mathbf{0} & \mathbf{V}^{-1} \end{bmatrix} \boldsymbol{x}'}_{\tilde{\boldsymbol{x}}'} = \begin{bmatrix} \mathbf{0} & \mathbf{I} \\ \mathbf{\Lambda} & \mathbf{0} \end{bmatrix} \underbrace{\begin{bmatrix} \mathbf{V}^{-1} & \mathbf{0} \\ \mathbf{0} & \mathbf{V}^{-1} \end{bmatrix} (\boldsymbol{x} - \boldsymbol{x}_e)}_{\tilde{\boldsymbol{x}} - \tilde{\boldsymbol{x}}_e}.$$

By defining a transformed state vector, $\tilde{\boldsymbol{x}}$, we reduce our linearized state equations to

$$\tilde{\boldsymbol{x}}' = \underbrace{\begin{bmatrix} \mathbf{0} & \mathbf{I} \\ \mathbf{\Lambda} & \mathbf{0} \end{bmatrix}}_{\mathbf{\Psi}} (\tilde{\boldsymbol{x}} - \tilde{\boldsymbol{x}}_e). \tag{15}$$

Equation (15) has the general solution

$$\tilde{\boldsymbol{x}} = e^{\mathbf{\Psi} s} \boldsymbol{c} + \tilde{\boldsymbol{x}}_e, \quad \boldsymbol{c} = \begin{bmatrix} \boldsymbol{c}_1 \\ \boldsymbol{c}_2 \end{bmatrix}, \quad \tilde{\boldsymbol{x}}_e = \begin{bmatrix} \tilde{\boldsymbol{\theta}}_e \\ \mathbf{0} \end{bmatrix},$$

where $\boldsymbol{c}$ is a vector of constants determined by the boundary conditions. The proximal boundary from (10) evaluates to $\mathbf{V}\boldsymbol{c}_1 + \beta_\sigma \mathbf{V}\boldsymbol{c}_2 = \mathbf{0}$, while the distal boundary relies on the fact that

$$e^{\mathbf{\Psi} L} = \begin{bmatrix} \cosh(L\sqrt{\mathbf{\Lambda}}) & (\sqrt{\mathbf{\Lambda}})^{-1} \sinh(L\sqrt{\mathbf{\Lambda}}) \\ \sqrt{\mathbf{\Lambda}} \sinh(L\sqrt{\mathbf{\Lambda}}) & \cosh(L\sqrt{\mathbf{\Lambda}}) \end{bmatrix},$$

and evaluates to[2]

$$\mathbf{V}\sqrt{\mathbf{\Lambda}} \sinh(L\sqrt{\mathbf{\Lambda}})\boldsymbol{c}_1 + \mathbf{V} \cosh(L\sqrt{\mathbf{\Lambda}})\boldsymbol{c}_2 = \mathbf{0}. \tag{16}$$

The proximal boundary imposes the constraint $\boldsymbol{c}_1 = -\beta \boldsymbol{c}_2$, which can be substituted into (16) to produce

$$\mathbf{V} \underbrace{\left[\cosh(L\sqrt{\mathbf{\Lambda}}) - \beta\sqrt{\mathbf{\Lambda}} \sinh(L\sqrt{\mathbf{\Lambda}}) \right]}_{\mathbf{T}} \boldsymbol{c}_2 = \mathbf{0}.$$

This equation has a non-trivial solution, $\tilde{\boldsymbol{x}} \neq \tilde{\boldsymbol{x}}_e$, when the matrix $\mathbf{T}$ drops rank. Since $\mathbf{\Lambda}$ is diagonal, this is equivalent to determining when any diagonal element of $\mathbf{T}$ is zero. Therefore, $\boldsymbol{\theta}_e$ bifurcates when:

$$\beta = \frac{\coth(L\sqrt{\lambda_j})}{\sqrt{\lambda_j}} \tag{17}$$

for any λ_j, where λ_j is the j^{th} eigenvalue of $\mathbf{A}_e$. This equation is only solvable for $\lambda_j < 0$ (since $\beta \leq 0$). When $\beta = 0$, this condition requires $L^2 \lambda_j = -\frac{\pi^2}{4}$, which is a generalization of the condition shown in the literature for two tubes. Indeed, comparing (17) to (8), it is clear that the bifurcation theory generalizes nicely to n tubes (the sign difference and cot/coth is due to the sign of λ_j, and in (8) L is lumped into λ_0).

B. Unequal Transmission Lengths

Analogous to the extension from two tubes, torsional equilibrium, or $\sum_{j=1}^{n} k_{jt} \psi_j' = 0$, creates a relationship between the absolute torsion and the relative torsion

$$\psi_i' = \frac{1}{k_t} \sum_{j=1}^{n} k_{jt}(\theta_i' - \theta_j'), \quad k_t = \sum_{j=1}^{n} k_{jt}. \tag{18}$$

The proximal boundary condition with unequal transmission lengths is $\theta_i(0) = \alpha_i - \alpha_1 - \beta_i \psi_i'(0) + \beta_1 \psi_1'(0)$, and can be re-expressed using (18) in terms of relative angles as

$$\theta_i(0) = \alpha_i - \alpha_1 - \beta_i \theta_i'(0) + \frac{\beta_i - \beta_1}{k_t} \sum_{j=1}^{n} k_{jt} \theta_j'(0).$$

Since this expression is linear in θ_i', we define the matrix $\mathbf{B}$ as

$$\mathbf{B}(i-1, j-1) = \begin{cases} \dfrac{\beta_1 - \beta_i}{k_t} k_{it} + \beta_i & (i = j) \\ \dfrac{\beta_1 - \beta_i}{k_t} k_{jt} & (i \neq j) \end{cases} \tag{19}$$

for $i, j = 2, \ldots, n$. Using $\mathbf{B}$, the proximal boundary condition can be expressed as

$$\boldsymbol{\theta}(0) = \boldsymbol{\theta}_e - \mathbf{B}\boldsymbol{\theta}'(0), \tag{20}$$

[1] The Jacobian of (2) at an equilibrium, in the variables ψ_i, is similar to a symmetric matrix and therefore nondefective. It can then be shown that the transformation to the $(n-1)$ dimensional subspace corresponding to the variables θ_i retains a complete basis of eigenvectors for its Jacobian, $\mathbf{A}_e$.

[2] cosh and sinh are defined here by the Taylor series expansion for the matrix arguments.

and the distal boundary condition remains unchanged from (16). Evaluation of the proximal boundary condition gives $\mathbf{V}\boldsymbol{c}_1 + \mathbf{B}\mathbf{V}\boldsymbol{c}_2 = \mathbf{0}$, which provides the constraint that $\boldsymbol{c}_1 = -\mathbf{V}^{-1}\mathbf{B}\mathbf{V}\boldsymbol{c}_2$. After substituting into (16), we have

$$\underbrace{\mathbf{V}\left(\cosh(L\sqrt{\mathbf{\Lambda}}) - \sqrt{\mathbf{\Lambda}}\sinh(L\sqrt{\mathbf{\Lambda}})\mathbf{V}^{-1}\mathbf{B}\mathbf{V}\right)}_{\mathbf{T}^*}\boldsymbol{c}_2 = \mathbf{0}.$$

Therefore, $\boldsymbol{\theta}_e$ bifurcates when the matrix $\mathbf{T}^*$ drops rank, or equivalently, when $\det(\mathbf{T}^*) = 0$.

V. Maximum Snap-Free Tube Overlap: Three Tube Analysis

In [12], a canonical case for two fully overlapped tubes is described, where each tube is assumed to have the same stiffness, be made of the same material, have no transmission length, and have equal curvature. In this case, the bifurcation parameter simplifies to $\lambda = L^2\kappa^2(1+\nu)$. The tube overlap angle was defined as $\gamma = L\kappa$, so $\lambda = \gamma^2(1+\nu)$. Assuming the concentric tube robot is made of nitinol tubes, Poisson's ratio is approximately $\nu = 0.3$ [12]. Thus, the critical snap-free tube overlap angle γ_c was shown to be

$$\gamma_c = \sqrt{\frac{\lambda_0}{1+\nu}} = \frac{\pi}{2\sqrt{1+\nu}} = 1.38 \text{ rad}, \ 79^\circ.$$

Using the techniques from Section IV, we can extend this result to three tubes. Note that the purpose of this example is not to produce a practical physical prototype, but rather to show that several model special cases that have been previously observed in the two-tube model generalize.

With the same canonical assumptions of identical, fully overlapping tubes, each coefficient in (13) $\mathbf{\Phi}_{ij} = \Phi$, where $\Phi = \kappa^2\frac{1+\nu}{3}$. For three tubes, there are six equilibria in the domain $\theta_i \in [0, 2\pi)$: $\boldsymbol{\theta}_e^T = \begin{bmatrix}0 & 0\end{bmatrix}$, $\begin{bmatrix}\pi & 0\end{bmatrix}$, $\begin{bmatrix}0 & \pi\end{bmatrix}$, $\begin{bmatrix}\pi & \pi\end{bmatrix}$, $\begin{bmatrix}2\pi/3 & 4\pi/3\end{bmatrix}$, and $\begin{bmatrix}4\pi/3 & 2\pi/3\end{bmatrix}$. However, with our assumptions of equal stiffness and curvature, several of these cases are clearly equivalent, so we can reduce the set to $\boldsymbol{\theta}_e^T = \begin{bmatrix}0 & 0\end{bmatrix}$, $\begin{bmatrix}\pi & 0\end{bmatrix}$, $\begin{bmatrix}2\pi/3 & 4\pi/3\end{bmatrix}$.

The equilibrium $\boldsymbol{\theta}_e^T = \begin{bmatrix}0 & 0\end{bmatrix}$ represents all three tubes aligned with one another, with the same direction of precurvature. The matrix $\mathbf{A}_e$ of (13) for this case has all positive eigenvalues ($\lambda_{1,2} = 3\Phi$), which we have shown precludes a bifurcation point.

The equilibrium $\boldsymbol{\theta}_e^T = \begin{bmatrix}\pi & 0\end{bmatrix}$ represents one tube rotated 180° from the other two tubes. For this case, the eigenvalues of $\mathbf{A}_e$ are $\lambda_1 = -3\Phi$, $\lambda_2 = \Phi$. Recall, with $\beta = 0$, the critical bifurcation parameter for n tubes is $\lambda_0 = \frac{-\pi^2}{4}$. By equating $L^2\lambda_1$ to the critical bifurcation parameter, the maximum snap-free tube overlap angle, γ_c, can be determined. We have that $-3L^2\Phi = -\gamma_c^2(1+\nu) = \frac{-\pi^2}{4}$, or $\gamma_c = \frac{\pi}{2\sqrt{1+\nu}} = 1.38$ rad, or 79°. Remarkably, this implies that the design constraints on the tube parameters that prevent snapping are unchanged when moving from two to three tubes.

The final equilibrium to evaluate, which does not have an analogy for two tubes, is $\boldsymbol{\theta}_e^T = \begin{bmatrix}2\pi/3 & 4\pi/3\end{bmatrix}$. This represents the three tubes all rotated 120° from each other. Intuitively, this trivial solution will straighten out the combined set of tubes unless a non-trivial, energetically favorable solution branch exists. At this equilibrium, the eigenvalues of $\mathbf{A}_e$ evaluate to $\lambda_{1,2} = -1.5\Phi$. Equating $-1.5L^2\Phi$ to λ_0, we find the critical angle of snap-free tube overlap angle to be $\gamma_c = \frac{\sqrt{2}\pi}{2\sqrt{1+\nu}} = 1.95$ rad, or 112°. This equilibrium bifurcates at a much larger γ_c, which demonstrates that a bifurcation of one equilibrium does not imply bifurcation of all equilibria. However, a configuration can be deemed snap-free by ensuring that none of the equilibria have bifurcated.

Although we have not proven this, we have found in simulation that these $\gamma_c = 79^\circ$ and $\gamma_c = 112^\circ$ results extend to an arbitrary number of tubes for these canonical conditions. The equilibrium $\boldsymbol{\theta}_e$, where each element is either 0 or π, with at least one element π (which is always an equilibrium), will bifurcate at $\gamma_c = 79^\circ$, regardless of the number of tubes. Similarly, the equilibrium that exists for more than two tubes where each tube is rotated $\frac{360^\circ}{n}$ from adjacent tubes bifurcates at $\gamma_c = 112^\circ$, regardless of the number of tubes.

VI. Design Implications and Implementation

A. Transmission Lengths

From equations (8), (17), and Fig. 6, it is clear that transmission lengths, which are often an afterthought of tube design, are important to consider for guaranteed elastic stability. The designer should consider ways to reduce these lengths, if possible. Alternatively, if the transmission sections are not required to be elastic, replacing these sections with stiffer sections will enhance the stability of the design. In general, preventing unnecessary strain energy build up in the backbone of the robot should be prioritized for elastic stability.

B. Two Tube Snap-Free Design Space: Implementation

Design optimization problems often seek to maximize the robot's workspace, or to optimally match the workspace to a task, subject to a set of constraints [1], [6]. The snapping problem can be taken as another constraint, and the designer can reduce the potential design space by excluding designs which can snap. Algorithm 1 provides a method to reduce a potential two-tube design space to a subspace that is snap-free. Note that, given a translational configuration of the robot and all of the tube parameters, the inner loop of Algorithm 1 provides a test for whether all rotational configurations are snap-free.

C. A Several Tube Snap Test: Implementation

While canonical cases are useful for gaining intuition, in practice, the robot backbone will typically contain several distinct sections where the number of tubes and precurvature of each is constant. The analysis from Section IV can accommodate these conditions as follows.

Algorithm 1 The snap-free design space for two tubes

Input: All possible tube precurvatures: K
Tube parameters (geometry, material, lengths): p
Maximum precurved tube overlap: L_{max}
Output: Snap-free design space: D

```
for L = 0 to L_max do
  for all κ1, κ2 ∈ K do
    β1, β2 ← Fig. 1 using p
    λ ← Eq. (5) using p, L, κ1, κ2
    if λ < π²/4 then
      β_eq,σ ← Eq. (9) using β1, β2, p, L
      bifurcate ← (β_eq,σ + cot(√λ)λ^{-1/2} ≤ 0) {Eq. (8)}
      if bifurcate = false or λ = 0 then
        Add [κ1, κ2, L] to D
      end if
    end if
  end for
end for
```

1) Finding Equilibria: Finding equilibria is actually usually simpler in general cases than in fully overlapped cases, since there are fewer equilibria to consider. Recall that an equilibrium must be a fixed point that solves (10) for all s. In a physical robot, even if it is composed of several tubes, there will almost always be a section where only two tubes are present. The only equilibria in the two tube section are $\theta_e = 0, \pi$, and since any candidate equilibrium point must hold for all sections simultaneously, we need not consider all permutations of tube angles for sections with more than two tubes. This means the only $\boldsymbol{\theta}_e$ that need to be considered are composed of only zero and π elements, with at least one element π. Therefore, for an n tube robot, the designer need only to consider $2^{n-1}-1$ equilibria. We have found in a large number of simulations that the additional equilibria that arise in the special-case, fully overlapped configurations bifurcate at larger critical bifurcation parameters.

2) Defining Nodes and Sections: We define a node as any arc length along the robot where there is a discontinuity in (i) the number of tubes present or (ii) the precurvature of any of the tubes. For tubes that are straight with a constant curvature section, a node will exist where the straight section terminates. We define a section as connecting consecutive nodes. A given robot configuration will have $m+1$ nodes, and m sections. To start, define node N_0 at the most proximal arc length where at least two precurved tubes overlap, and set this arc length to $N_0 = 0$. Next, define N_m as the most distal arc length where at least two tubes are present. Define all remaining nodes, $N_1, \ldots, N_{m-1}$ from proximal to distal between N_0 and N_m. We use the convention that section k connects nodes N_{k-1} and N_k.

3) Propagating Linearized Solutions Through Sections: An $n \times n$ parameter matrix, $\boldsymbol{\Phi}_k$, can be defined for the k^{th} section from (11). If tube i is not present in the section, set $k_{ib} = 0$, which must also be enforced when calculating k_b. Using $\boldsymbol{\Phi}_k$ and the equilibrium $\boldsymbol{\theta}_e$, calculate $\tilde{\mathbf{A}}_{e,k}$ from (13) and (14), which is $\tilde{\mathbf{A}}_e$ for section k. The sum from (13) is computed over the total tubes present in the entire robot, regardless of the section. Without loss of generality, assume in (14) that the equilibrium is at $\boldsymbol{\theta}_e = \mathbf{0}$ (a change of variables can always achieve this). The solution to (14) for section k is $\boldsymbol{x}(s) = e^{\tilde{\mathbf{A}}_{e,k}(s-N_{k-1})}\boldsymbol{x}(N_{k-1})$ for $N_{k-1} \le s \le N_k$. By assuming that $k_{ib} = 0$ when tubes are no longer present, the distal boundary conditions are all implicitly extended to the most distal node, N_m. At the distal node of the first section, we have that $\boldsymbol{x}(N_1) = e^{\tilde{\mathbf{A}}_{e,1}N_1}\boldsymbol{x}(0)$. At the distal node of the second section, we have that $\boldsymbol{x}(N_2) = e^{\tilde{\mathbf{A}}_{e,2}(N_2-N_1)}\boldsymbol{x}(N_1)$, and substituting, we have that $\boldsymbol{x}(N_2) = e^{\tilde{\mathbf{A}}_{e,2}(N_2-N_1)}e^{\tilde{\mathbf{A}}_{e,1}N_1}\boldsymbol{x}(0)$. This process propagates through the sections until the final node, N_m, is reached, so we have $\boldsymbol{x}(N_m) = \mathbf{H}\boldsymbol{x}(0)$ where

$$\mathbf{H} = e^{\tilde{\mathbf{A}}_{e,m}(N_m-N_{m-1})}\ldots e^{\tilde{\mathbf{A}}_{e,1}(N_1-N_0)}. \tag{21}$$

4) Finding Bifurcation Points: Since the state $\boldsymbol{x}(0) = \begin{bmatrix}\boldsymbol{\theta}(0) & \boldsymbol{\theta}'(0)\end{bmatrix}^T$, and $\boldsymbol{\theta}(0) = -\mathbf{B}\boldsymbol{\theta}'(0)$ from (20), we can simplify $\boldsymbol{x}(N_m) = \mathbf{H}\boldsymbol{x}(0)$ to

$$\begin{bmatrix}\boldsymbol{\theta}\\ \boldsymbol{\theta}'\end{bmatrix}(N_m) = \underbrace{\mathbf{H}\begin{bmatrix}-\mathbf{B}\\ \mathbf{I}\end{bmatrix}}_{\mathbf{S}}\boldsymbol{\theta}'(0). \tag{22}$$

We have reformulated the several point boundary value problem to a two point boundary via this propagation and now have $\boldsymbol{\theta}'(N_m) = \mathbf{0}$, or

$$\boldsymbol{\theta}'(N_m) = \mathbf{S}_2\boldsymbol{\theta}'(0) = \mathbf{0}, \tag{23}$$

where $\mathbf{S}_2$ is the $(n-1)\times(n-1)$ matrix extracted from the bottom half of $\mathbf{S}$. If a non-trivial solution with $\boldsymbol{\theta}'(0) \neq 0$ can be found, then this indicates a bifurcation point and hence the possibility that the robot could snap between configurations. If $\mathbf{S}_2$ is full rank, then the only solution to (23) is the trivial, equilibrium solution $\boldsymbol{\theta}'(0) = \mathbf{0}$. However, when $\det(\mathbf{S}_2) = 0$, a non-trivial solution exists and the equilibrium bifurcates.

As tube parameters and translational actuation is smoothly varied, the determinant will vary in a smooth way, even across a bifurcation point. We know that $\det(\mathbf{S}_2) > 0$ for non-bifurcated configurations (this can be shown in several ways; for example, when all tubes are straight, we have $\mathbf{S}_2 = I$), so any configuration with $\det(\mathbf{S}_2) \le 0$ indicates the equilibrium configuration assessed has bifurcated. We note that $\det(\mathbf{S}_2) = 0$ at every mode of bifurcation, but from a practical standpoint, any realistic robot will not be near the second mode of bifurcation, so searching for $\det(\mathbf{S}_2) \le 0$ will suffice. It is good practice, however, to initialize a simulation in a known stable configuration and vary parameters from this configuration. Algorithm 2 gives a test to determine if a robot in any configuration, composed of any number of tubes, could snap.

D. Design Space Reduction Example

There are typically many parameters available in concentric tube robot design. These include the number of tubes, their diameters, curvature of each, and lengths of curved and straight sections. If these parameter ranges are sampled at even a moderately fine discretization, a brute force search is undesirable due to the beam mechanics model that must be solved for each workspace point considered for each design.

Algorithm 2 The several tube snapping criterion

Input: Tube parameters p and translational actuation
All equilibria: $\{e_1, \ldots, e_n\} \in e$
Output: Bifurcation: **true/false**

$m+1$ nodes, m sections $\leftarrow$ using translational actuation, p
$\beta_1, \ldots, \beta_n \leftarrow$ using translational actuation, p
$\mathbf{B} \leftarrow$ Eq. (19) using $\beta_1, \ldots, \beta_n, p$
for $k = 1$ to m **do**
  $\mathbf{\Phi}_k \leftarrow$ Eq. (11) using p
end for
for all e **do**
  for $k = 1$ to m **do**
    $\tilde{\mathbf{A}}_{e,k} \leftarrow$ Eq. (13), (14) using $\mathbf{\Phi}_k, e$
  end for
  $\mathbf{H} \leftarrow$ Eq. (21) using $\tilde{\mathbf{A}}_{e,1}, \ldots, \tilde{\mathbf{A}}_{e,m}$.
  $\mathbf{S}_2 \leftarrow$ Eq. (22) using $\mathbf{H}, \mathbf{B}$.
  if $\det(\mathbf{S}_2) \leq 0$ **then**
    return true
  end if
end for
return false

TABLE I: Simulation Tube Parameters (mm)

Tube	OD	ID	Straight Length	Curved Length
Inner	1.16	0.86	170	40
Middle	1.64	1.34	125	40
Outer	2.86	1.86	80	40

The purpose of Algorithm 2 is to eliminate many designs from consideration a priori. As an example, consider the simple robot from [1] consisting of a straight, rigid outer tube, and two curved inner tubes. To simplify the problem, assume that tube diameters and straight and curved section lengths, are as shown in Table I, with Poisson's ratio 0.3 and Young's Modulus 50 GPa. For this simulation, we allow the outer tube to be curved, so the remaining design space consists of the precurvature of each tube, and here we consider a (physically realizable) range of $[2, 30]$ m^{-1} for each. Discretizing these ranges into $N = 20$ evenly spaced values, the design space is composed of $N^3 = 8000$ total combinations. Fortunately, Algorithm 2 can be used to help the designer only search over a subset of these. Before applying it, we make one final assumption (again conservative, simply for ease of computation of this example), which is that no outer tube extends past the tip of a tube within it, and that we extend the tubes 40 mm.

Using translational steps of 2.5 mm for each tube, we applied Algorithm 2. If during a step Algorithm 2 returned a bifurcation, the design was eliminated. Of the 8000 total potential designs, 7179 of them had snaps somewhere in their workspace. Thus, Algorithm 2 reduced the design space by approximately 90%. Note that the benefit of reducing the design space would become even more pronounced if one allowed the number of tubes to vary, as well as other parameters like the lengths of the curved sections of the tubes.

VII. Conclusion

We have presented a framework which can be used to design concentric tube robots (composed of any number of tubes, with transmission lengths) that will not snap during actuation in free space. We have also shown that the snapping phenomenon can be analyzed using local bifurcation theory. The results derived in this paper can provide design and actuation constraints for the constant curvature robots that are most often employed today and can be included into future design optimization and motion planning algorithms.

References

[1] J. Burgner, H. B. Gilbert, and R. J. Webster III, "On the computational design of concentric tube robots: Incorporating volume-based objectives," *IEEE International Conference on Robotics and Automation*, pp. 1185–1190, 2013.

[2] H. B. Gilbert, D. C. Rucker, and R. J. Webster III, "Concentric tube robots: State of the art and future directions," in *16th International Symposium on Robotics Research (2013). Springer Tracts in Advanced Robotics*, In Press.

[3] R. Xu, S. F. Atashzar, and R. V. Patel, "Kinematic instability in concentric-tube robots: Modeling and analysis," *IEEE International Conference on Biomedical Robotics and Biomechatronics*, 2014.

[4] C. Bergeles and P. E. Dupont, "Planning stable paths for concentric tube robots," *IEEE/RSJ International Conference on Intelligent Robots and Systems*, pp. 3077–3082, 2013.

[5] T. Anor, J. R. Madsen, and P. Dupont, "Algorithms for design of continuum robots using the concentric tubes approach: a neurosurgical example," in *IEEE International Conference on Robotics and Automation*, 2011, pp. 667–673.

[6] C. Bedell, J. Lock, A. Gosline, and P. E. Dupont, "Design optimization of concentric tube robots based on task and anatomical constraints," *IEEE International Conference on Robotics and Automation*, pp. 398–403, 2011.

[7] J. Burgner, P. J. Swaney, D. C. Rucker, H. B. Gilbert, S. T. Nill *et al.*, "A bimanual teleoperated system for endonasal skull base surgery," in *IEEE/RSJ International Conference on Intelligent Robots and Systems*, 2011, pp. 2517–2523.

[8] L. A. Lyons, R. J. Webster III, and R. Alterovitz, "Planning Active Cannula Configurations Through Tubular Anatomy," in *IEEE International Conference on Robotics and Automation*, 2010, pp. 2082–2087.

[9] J. Burgner-Kahrs, H. B. Gilbert, J. Granna, P. J. Swaney, and R. J. Webster III, "Workspace Characterization for Concentric Tube Continuum Robots," in *IEEE/RSJ International Conference on Intelligent Robots and Systems*, 2014, pp. 1269–1275.

[10] R. J. Webster III, J. M. Romano, and N. J. Cowan, "Mechanics of precurved-tube continuum robots," *IEEE Transactions on Robotics*, vol. 25, no. 1, pp. 67–78, 2009.

[11] R. J. Webster III, J. M. Romano, and N. J. Cowan, "Kinematics and calibration of active cannulas," *IEEE International Conference on Robotics and Automation*, pp. 3888–3895, 2008.

[12] P. E. Dupont, J. Lock, B. Itkowitz, and E. Butler, "Design and control of concentric-tube robots," *IEEE Transactions on Robotics*, vol. 26, no. 2, pp. 209–225, 2010.

[13] D. C. Rucker, B. A. Jones, and R. J. Webster III, "A geometrically exact model for externally loaded concentric tube continuum robots," *IEEE Transactions on Robotics*, vol. 26, pp. 769–780, 2010.

[14] J. Kim, D. Lee, K. Kim, S. Kang, and K. Cho, "Toward a solution to the snapping problem in a concentric-tube continuum robot: Grooved tubes with anisotropy," *IEEE International Conference on Robotics and Automation*, pp. 5871–5876, 2014.

[15] H. Azimian, P. Francis, T. Looi, and J. Drake, "Structurally-redesigned concentric-tube manipulators with improved stability," *IEEE/RSJ International Conference on Intelligent Robots and Systems*, 2014.

[16] J. Ha, F. Park, and P. Dupont, "Achieving elastic stability of concentric tube robots through optimization of tube precurvature," *IEEE/RSJ International Conference on Intelligent Robots and Systems*, 2014.

[17] J. Guckenheimer and P. Holmes, *Nonlinear Oscillations, Dynamical Systems, and Bifurcations of Vector Fields*. Springer-Verlag, 1983.

[18] S. S. Antman, *Nonlinear Problems of Elasticity*, 2nd ed. Springer-Verlag, 2005.

[19] D. C. Rucker, "The mechanics of continuum robots: Model-based sensing and control," Ph.D. dissertation, Vanderbilt University, 2011.